

## Periodic and Disordered Structures in a Modulated Gas-Driven Granular Layer

J. Li,<sup>1</sup> I. S. Aranson,<sup>1</sup> W.-K. Kwok,<sup>1</sup> and L. S. Tsimring<sup>2</sup>

<sup>1</sup>Argonne National Laboratory, 9700 South Cass Avenue, Argonne, Illinois 60439

<sup>2</sup>Institute of Nonlinear Science, University of California–San Diego, La Jolla, California 92093-0402  
(Received 9 December 2002; revised manuscript received 10 February 2003; published 2 April 2003)

Experiments with a thin gas-fluidized granular layer revealed a sequence of well-defined transitions as the amplitude and frequency of the gas flow modulation are varied. The observed patterns include subharmonic squares and stripes, quasiperiodic and disordered structures. The wavelength of subharmonic patterns increases with the mean flow rate and decreases with the modulation frequency.

DOI: 10.1103/PhysRevLett.90.134301

PACS numbers: 45.70.Mg, 45.70.Qj

Gas-fluidized beds are widely used in industry for mixing, catalysis, combustion, and other applications. Their properties are the subject of intensive research [1]. In most industrial realizations, a fluidized bed consists of a vertical column energized by the flow of gas or liquid pumped through the bottom via a certain distributor system. Fluidization occurs when the drag force exerted by the fluid on the granulate exceeds gravity. A uniform fluidization, the most desirable regime for most industrial application, turns out to be prone to bubbling instability: Bubbles of clear fluid created at the bottom traverse the granular layer and destroy the uniform state [2,3]. The study of mechanisms of bed instabilities is an active research area in the engineering community. Current fluidization studies mainly focus on thick fluidized beds where the thickness of the granular layer is much larger than the horizontal dimensions. Experimental analysis of thick fluidized beds is greatly impeded by the difficulty in controlling and monitoring the bubbling processes in the bulk of the bed, although progress has been made with the help of certain noninvasive techniques [4]. Less attention is devoted to shallow fluidized beds due to their perceived lesser technological importance. However, layered beds have promising industrial applications [5]. Spontaneous pressure oscillations and some aspects of the shallow bed dynamics were studied in Refs. [6–8].

In this Letter, we report experimental studies of thin granular layer fluidization by periodically modulated gas flow. Mechanical vibration is often used to improve fluidization of fine powders which is frequently hampered by the formation of channels through which the fluid escapes [9]. However, induced mechanical excitation near the walls is very energy consuming and propagates only a few centimeters into the bulk and, consequently, is not effective in large systems. We demonstrate that modulation of the air flow can serve as an alternative and more effective way of imparting vibrations on the granular particles in the bulk of the bed. Moreover, a shallow bed geometry allows us to study the spatiotemporal dynamics of the bed under periodic gas modulations. We find a sequence of well-defined transitions between disordered states dominated by spontaneous bubbling fluidization to

ordered periodic subharmonic patterns as the frequency, the amplitude of modulation, and the flow rate are varied. The observed ordered states include periodic squares and stripes and some more complicated structures. The pattern wavelength is determined by the frequency of the modulation and the mean flow rate. The transition to periodic patterns is associated with a decrease of pressure drop across the bed, suppression of large bubble formation, and the expansion of the controllable fluidization regime.

A schematic of the experiment is shown in Fig. 1. The cell is built of transparent Plexiglas and has an inner diameter of 140 mm. The granular layer thickness  $h$  was varied from 3 to 12 mm. We typically used 0.15 mm diameter bronze spheres or 0.2 mm glass beads (both powders correspond to Geldart B type [10]). Similar results were obtained for other Geldart B type particles. The bottom of the bed is made of a sintered porous brass plate with an average pore size of 60  $\mu\text{m}$ . Packed plastic

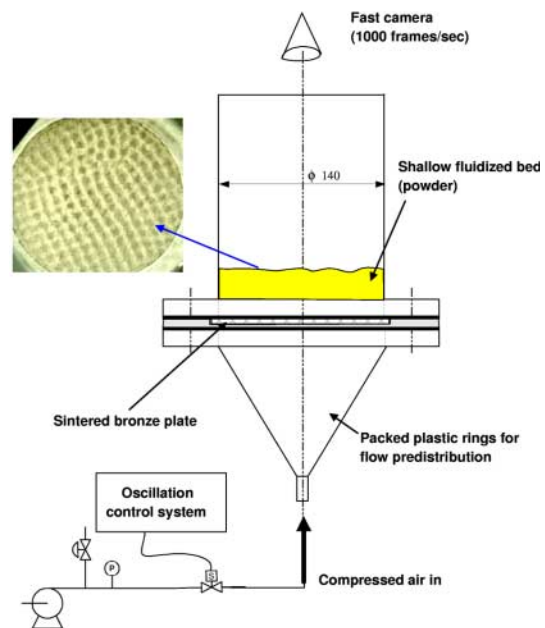


FIG. 1 (color online). Schematics of the experimental setup.

rings are used for flow redistribution. Dry air is pumped through the layer, and the flow rate is controlled by a proportional valve with response time below 4 msec. The mean flow rate was measured by a precision mass flow meter. The mean flow velocity  $\bar{U}$  was varied in the range 0–40 cm/sec and the frequency of modulation  $f_0$  was changed from 0 to 40 Hz. The instant flow velocity  $U$  was periodically modulated in time as

$$U = \bar{U} + U_{osc} \sin(2\pi f_0 t), \quad (1)$$

where  $U_{osc}$  is the amplitude of the flow velocity modulation. The surface images were collected using a high-speed digital camera (up to 1000 frames per second) suspended above the bed. The pressure drop  $\Delta p$  across the layer was monitored by a differential pressure sensor, and the data were processed by a digital spectrum analyzer. In the absence of ac driving, the bed exhibits spontaneous oscillations with two typical frequencies: The first one about 17–22 Hz (for  $h = 3$  mm) is due to homogeneous bed oscillations [6], and the second one  $f_1 \approx 30$ –35 Hz is due to air bubbling [7].

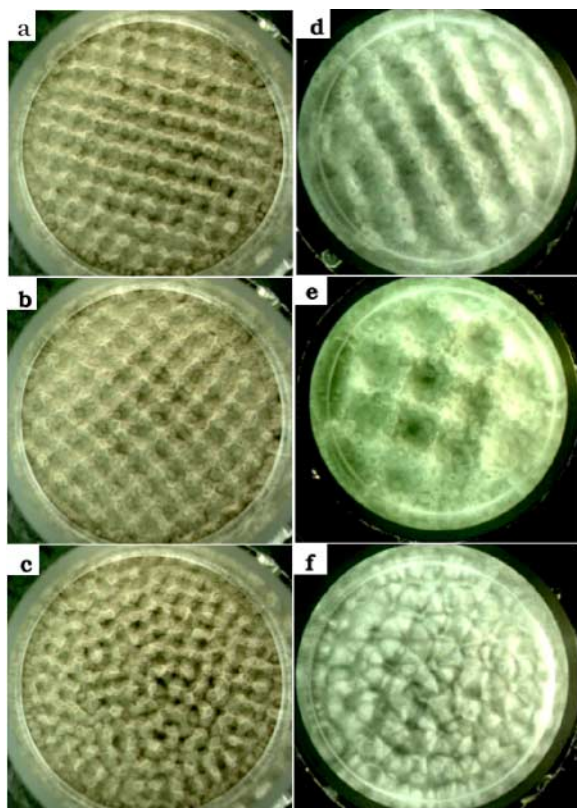


FIG. 2 (color online). Representative patterns for bronze particles (a)–(c) and glass beads (d)–(f). For (a)–(c), the parameters are  $h = 3$  mm,  $U_{osc} = 0.9\bar{U}$ ,  $\bar{U} = 3U_{mf}$ , and frequency  $f_0 = 22$  Hz (a),  $f_0 = 20$  Hz (b), and  $f_0 = 23$  Hz (c). For (d)–(f), the parameters are  $h = 6$  mm,  $U_{osc} = 0.9\bar{U}$ ,  $\bar{U} = 3.1U_{mf}$ , frequency  $f_0 = 16$  Hz (d),  $f_0 = 13.5$  (e), and  $f_0 = 20$  Hz (f). See also [11] for experimental animations.

The select patterns for various regimes of fluidization and different types of particles are shown in Fig. 2. The simplified phase diagram for bronze particles is shown in Fig. 3 [12]. A similar phase diagram is obtained for glass particles. The mean flow velocity and the amplitude of velocity modulation are measured in units of the minimal fluidization velocity  $U_{mf}$  ( $U_{mf} \approx 7$  cm/sec for bronze particles and  $U_{mf} \approx 2$  cm/sec for glass beads). Similar regimes were observed for different layer thicknesses. For small values of  $U_{osc}$ , the layer is practically flat, with only small-scale bubbles present. For higher  $U_{osc}$  values, stripes and squares are observed at higher and lower frequencies, respectively. Both stripes and squares are subharmonic, with two cycles of driving required to reproduce an original wave form. The transitions between patterns are rather sharp, with small or no hysteresis, except the line between squares and stripes where the transition is hard to identify due to additional transverse modulation of stripes. The corresponding power spectra  $S(f)$  of the pressure oscillations have a well-pronounced subharmonic peak at  $f_0/2$  (see Fig. 4). Typically, stripe patterns have transverse modulation [Fig. 2(a)] which we believe is due to the relatively high level of noise in the system (e.g., small-scale bubbling, effect of porous plate, etc.). This noise likely excites a transverse wave in the stripe regime, and also destroys long-range order in the case of square patterns.

Increasing the modulation frequency while keeping the mean flow rate fixed leads to a transition from squares or stripes to more disordered “quasi-hexagonal” patterns shown in Fig. 2(c). These “quasi-hexagons” have only short-range sixfold symmetry; i.e., each peak in the image is typically surrounded by six neighbors. While the spectrum of pressure oscillations for this pattern has a noticeable subharmonic component, the pattern is not

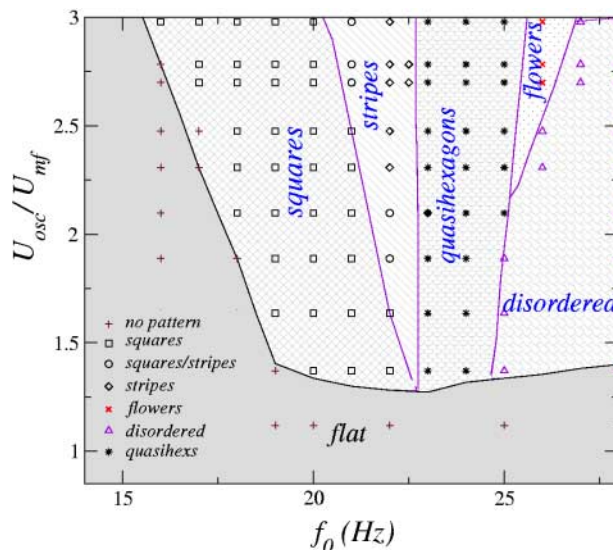


FIG. 3 (color online). Phase diagram,  $h = 3$  mm,  $\bar{U} = 3U_{mf}$ . Symbols show points where the measurements are taken.

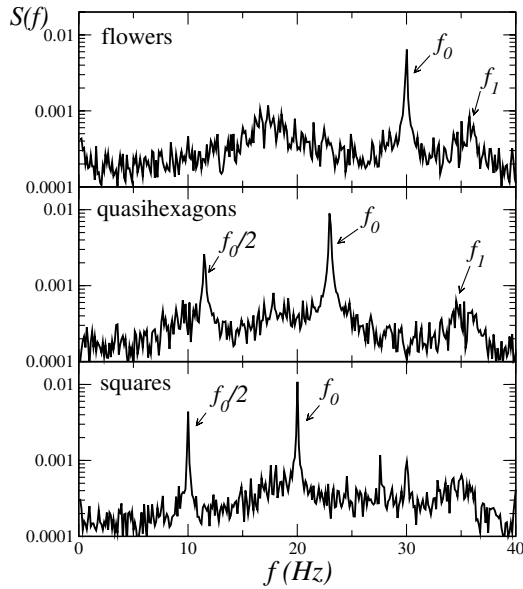


FIG. 4. Power spectra of pressure oscillations vs  $f$ :  $f_0$  denotes driving frequency;  $f_1$  indicates bubbling frequency. Mean flow rate is  $\bar{U} = 3U_{mf}$ , and amplitude of modulation  $U_{osc} = 0.9\bar{U}$ ,  $h = 3$  mm. Driving frequency  $f_0$  is 20 Hz for squares, 23 Hz for quasihexagons, and 30 Hz for flowers.

strictly periodic, and an additional peak corresponding to the air bubble formation frequency  $f_1$  appears in the spectrum. With further increase of  $f_0$ , the subharmonic component vanishes, and a flowerlike pattern appears [Fig. 2(f)], likely due to the interaction between the surface perturbation induced by the external modulation at the frequency  $f_0$  and the bubble formation (see Fig. 4). The “flower” size decreases with further increase of  $f_0$  and finally disappears, giving way to a disordered state. Whereas stripe and square patterns have direct analog in mechanically vibrated systems [13,14], quasi-hexagons and “flowers” are specific to the gas-driven system.

The dependence of the wavelength  $\lambda$  on the driving frequency  $f_0$  is shown in Fig. 5. For subharmonic squares and stripes, the wavelength monotonically decreases with the frequency. Remarkably, all the dependencies can be collapsed onto a single straight line in the rescaled variables  $\lambda/h$  vs  $1/hf_0^2$  (see inset of Fig. 5), yielding

$$\frac{\lambda}{h} = \Lambda_0 + \frac{\Gamma}{hf_0^2}, \quad (2)$$

where constants  $\Lambda_0 \approx 0.05$  and  $\Gamma \approx 0.5g$  do not depend on the bed thickness  $h$  ( $g$  is gravity acceleration). The frequency and the depth dependence of the dispersion relationship are similar to that of Refs. [13,15] for mechanically vibrated systems and gravitational waves on water surface [16]. However, there is a peak feature in the wavelength related to the transition from pure subharmonic patterns to more complicated ones (quasi-hexagons, flowers, etc.). We have found that an increase in the mean

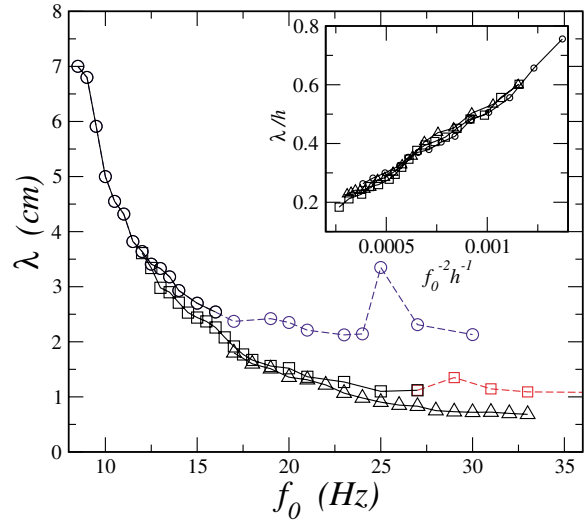


FIG. 5 (color online).  $\lambda$  vs  $f_0$ : bronze particles;  $\bar{U} = 3U_{mf}$ ,  $U_{osc} = 0.9\bar{U}$ ;  $\Delta$  correspond to  $h = 3$ ,  $\square$  to  $h = 6$ , and  $\circ$  to  $h = 9$  mm. Solid lines indicate subharmonic patterns (squares and stripes); dashed lines shows quasihexagons, flowers, and disordered. Inset:  $\lambda/h$  vs  $1/hf_0^2$  for subharmonic patterns.

flow rate leads to a small increase in the wavelength of the subharmonic patterns, likely due to the bed expansion with the increase of flow rate (see Fig. 6, inset). With the further increase of mean flow, the transition to quasi-hexagons occurs, associated with a decrease in the typical wavelength.

The mean pressure drop  $\langle \Delta p \rangle$  and the standard pressure drop deviation  $\zeta = \sqrt{\langle \Delta p^2 \rangle - \langle \Delta p \rangle^2}$  are shown in Fig. 6. In the range of frequencies corresponding to subharmonic patterns (squares and stripes), the mean pressure drop

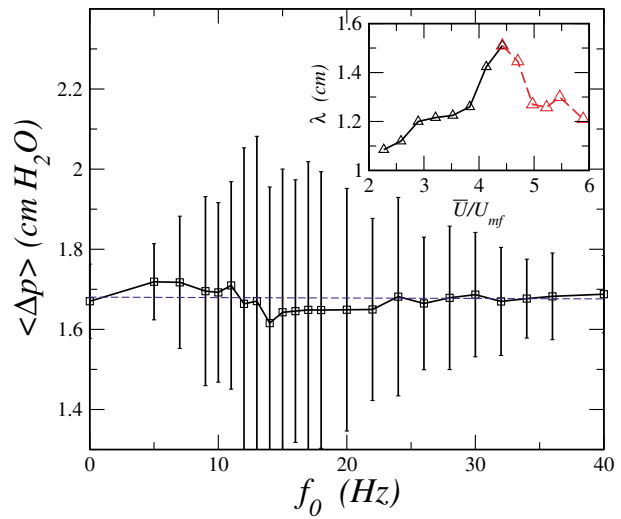


FIG. 6 (color online).  $\langle \Delta p \rangle$  vs  $f_0$ : Error bars show  $\zeta$ . Bronze particles;  $h = 6$  mm,  $U_{osc} = 0.9\bar{U}$ ,  $\bar{U} = 3U_{mf}$ . Inset:  $\lambda$  vs mean flow velocity  $\bar{U}/U_{mf}$  for  $h = 3$  mm,  $f_0 = 22$  Hz,  $U_{osc} = 0.9\bar{U}$ . Solid line corresponds to subharmonic squares and stripes; dashed line corresponds to “quasihexagons.”

displays a minimum whereas the pressure standard deviation shows a maximum ( $f_0 = 0$  shown by the dashed line corresponds to a conventional fluidized bed). Similar behavior was registered for different modulation amplitude values as well. The patterns survive up to a relatively high flow velocity  $6\bar{U}/U_{mf}$  (see inset of Fig. 6). For conventional fluidized beds, the bubbling occurs at a flow velocity of about  $1U_{mf}$  for Geldart B and D powder and  $3U_{mf}$  for Geldart A powder [10]. This opens up an opportunity to control gas-particle flow by utilizing flow modulation. Since bubbles in our system occur during the crest phase when the bed expands and their sizes are confined within the wavelength and layer thickness, a more efficient gas-solid contact is achieved. The alternative motion between the adjacent trough and crest produces strong shear, which could destroy the interparticle contacts.

Theoretical investigations of the pattern formation in vertically vibrated granular layers have attracted significant attention [17–20]. Several types of theoretical descriptions were proposed, including amplitude equations for parametrically excited waves [17], coupled map lattices [18,19], and simplified hydrodynamic models [20]. Our phenomenological approach to vertically vibrated layers [17] based on the principal symmetry of the problem should be able to describe the gas-driven granular layer as well. In the latter case, the order parameter will correspond to the amplitude of the subharmonic component of the surface deformation, and the driving term will be related to the amplitude of the flow modulation. Moreover, variation of the mean flow rate can be interpreted as variation of the gravitational acceleration in the mechanical system, which gives an additional “knob” to control the state of the system.

In conclusion, we studied the fluidization of a thin granular layer driven by modulated gas flow. We discovered a sequence of well-defined transitions of patterns as the amplitude, the frequency of gas flow modulation, and the mean flow rate were varied. The pattern wavelength is determined by the modulation frequency and mean flow velocity. Our experiments show that pattern formation is associated with a decrease in mean pressure drop across the layer and with an increase in pressure fluctuations, which results in the suppression of big bubble formation and expansion of the regime of controllable fluidization. The flow modulation can be used in industrial fluidized beds for improvement of fluidization, especially of cohesive and very fine particles [21]. The dispersion relationship for the surface waves Eq. (2) and the phase diagram can be useful for testing/validation of numerical codes for multiphase flows.

The work is supported by the U.S. DOE, BES-Materials Sciences, Contracts No. W-31-109-ENG-38 and No. DE-FG03-95ER14516.

- [1] D. Kunii and O. Levenspiel, *Fluidization Engineering* (Butterworth, Boston, 1991), p. 491; J.R. Grace, A. A. Avidan, and T.M. Knowlton, *Circulating Fluidized Beds* (Blackie Academic & Professional, London, 1997), p. 585.
- [2] R. Jackson, in *Fluidization*, edited by J.F. Davidson, R. Clift, and D. Harrison (Academic, London, 1985).
- [3] B.J. Glasser, S. Sundaresan, and I.G. Kevrekidis, *Phys. Rev. Lett.* **81**, 1849 (1998).
- [4] N. Menon and D.J. Durian, *Phys. Rev. Lett.* **79**, 3407 (1997).
- [5] M. Kwauk, *Fluidization Idealized Systems with Applications* (Prentice-Hall, Englewood Cliffs, NJ, 1993), p. 286.
- [6] J.W. Hiby, *Proceedings of the International Symposium on Fluidization* (Netherlands University Press, Amsterdam 1967), p. 99; J. Verloop and P.M. Heertjes, *Chem. Eng. Sci.* **29**, 1035 (1974).
- [7] L. S. Tsimring, R. Ramaswamy, and P. Sherman, *Phys. Rev. E* **60**, 7126 (1999); D. K. Clark, L. S. Tsimring, and I. S. Aranson, nlin.PS/0005010.
- [8] Tapped and blown powders were studied by J. Duran, *Phys. Rev. Lett.* **84**, 5126 (2000); **87**, 254301 (2001).
- [9] R. Gupta and A. S. Mujumbar, *Can. J. Chem. Eng.* **58**, 332 (1980); W. Yi, W. Tang-Jie, Y. Yi, and J. Yong, *Powder Technol.* **127**, 196 (2002).
- [10] D. Geldart, *Powder Technol.* **7**, 285 (1973).
- [11] See EPAPS Document No. E-PRLTAO-90-045313 for experimental animations. A direct link to this document may be found in the online article’s HTML reference section. The document may also be reached via the EPAPS homepage (<http://www.aip.org/pubservs/epaps.html>) or from <ftp.aip.org> in the directory /epaps/. See the EPAPS homepage for more information.
- [12] Small islands of complicated regular patterns were also observed in the “disordered” part of the phase diagram but not elaborated here because of the lack of space.
- [13] F. Melo, P. Umbanhowar, and H. L. Swinney, *Phys. Rev. Lett.* **72**, 172 (1994); F. Melo, P. B. Umbanhowar, and H. L. Swinney, *Phys. Rev. Lett.* **75**, 3838 (1995); P. B. Umbanhowar, F. Melo, and H. L. Swinney, *Nature (London)* **382**, 793 (1996).
- [14] I. S. Aranson *et al.*, *Phys. Rev. Lett.* **82**, 731 (1999).
- [15] C. Bizon *et al.*, *Phys. Rev. Lett.* **80**, 57 (1998).
- [16] L. D. Landau and E. M. Lifshits, *Fluid Mechanics* (Pergamon, New York, 1987).
- [17] L. S. Tsimring and I. S. Aranson, *Phys. Rev. Lett.* **79**, 213 (1997); I. S. Aranson, L. S. Tsimring, and V. M. Vinokur, *Phys. Rev. E* **59**, 1327 (1999).
- [18] T. Shinbrot, *Nature (London)* **389**, 574 (1997).
- [19] S. C. Venkataramani and E. Ott, *Phys. Rev. Lett.* **80**, 3495 (1998).
- [20] D. H. Rothman, *Phys. Rev. E* **57**, 1239 (1998); E. Cerda, F. Melo, and S. Rica, *Phys. Rev. Lett.* **79**, 4570 (1997); J. Eggers and H. Riecke, *Phys. Rev. E* **59**, 4476 (1999); H.-K. Park and H.-T. Moon, *Phys. Rev. E* **65**, 051310 (2002).
- [21] J. M. Valverde, A. Castellanos, and M. A. S. Quintanilla, *Phys. Rev. Lett.* **86**, 3020 (2001).